

Rechargeable and LED-activated $\text{ZnGa}_2\text{O}_4:\text{Cr}^{3+}$ near-infrared persistent luminescence nanoprobe for background-free biodetection

- Supporting Information

Zhihao Zhou,^{abcd} Wei Zheng,^{ad*} Jintao Kong,^a Yan Liu,^{ad} Ping Huang,^a Shanyong Zhou,^a Zhuo Chen,^{ad} Jianlin Shi,^{cd} and Xueyuan Chen^{abcd*}

^aCAS Key Laboratory of Design and Assembly of Functional Nanostructures, and Fujian Provincial Key Laboratory of Nanomaterials, Fujian Institute of Research on the Structure of Matter, Chinese Academy of Sciences, Fuzhou, Fujian 350002, China.

^bSchool of Physical Science and Technology, Shanghai Tech University, Shanghai 201210, China.

^cState Key Laboratory of High Performance Ceramic and Superfine Microstructures, Shanghai Institute of Ceramics, Chinese Academy of Sciences, Shanghai 200050, China.

^dUniversity of Chinese Academy of Sciences, Beijing 100049, China.

Fax: +86-591-63179421; Tel: +86-591-63179421; E-mail: xchen@fjirsm.ac.cn or zhengwei@fjirsm.ac.cn

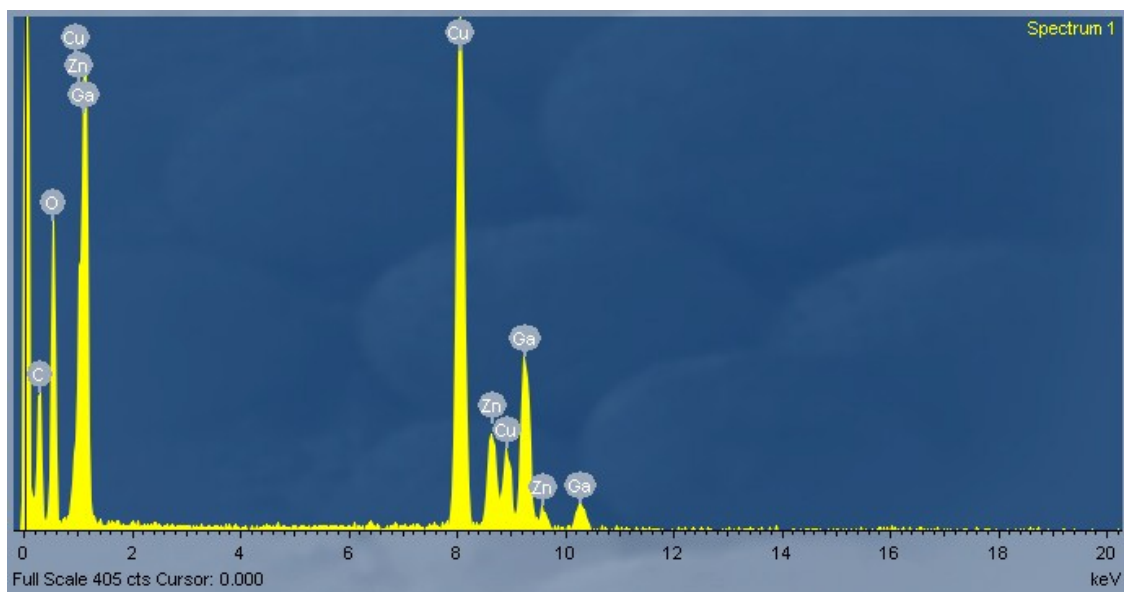


Figure S1. Energy dispersive X-ray spectrum (EDS) pattern showing the elements of Zn, Ga and O in the matrix of $\text{ZnGa}_2\text{O}_4:0.4\%\text{Cr}^{3+}$ PLNPs. The absence of the dopant Cr is due to its very low doping level of 0.4 mol% that cannot be detected by EDS.

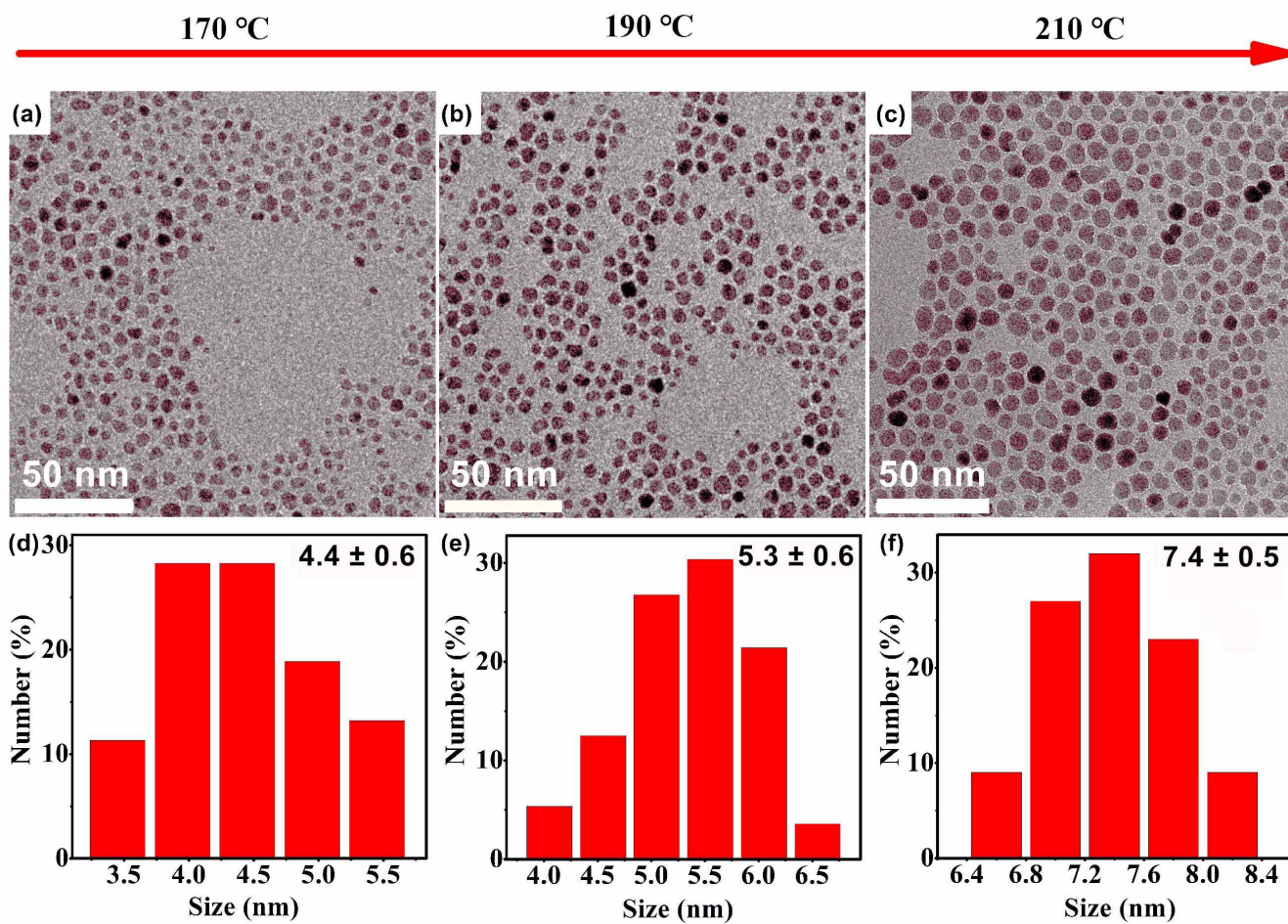


Figure S2. (a-c) TEM images and (d-f) size distribution of ZnGa₂O₄:0.4%Cr³⁺ PLNPs synthesized at different temperatures for 16 h. The size distribution was obtained by calculating 200 particles in the TEM images.

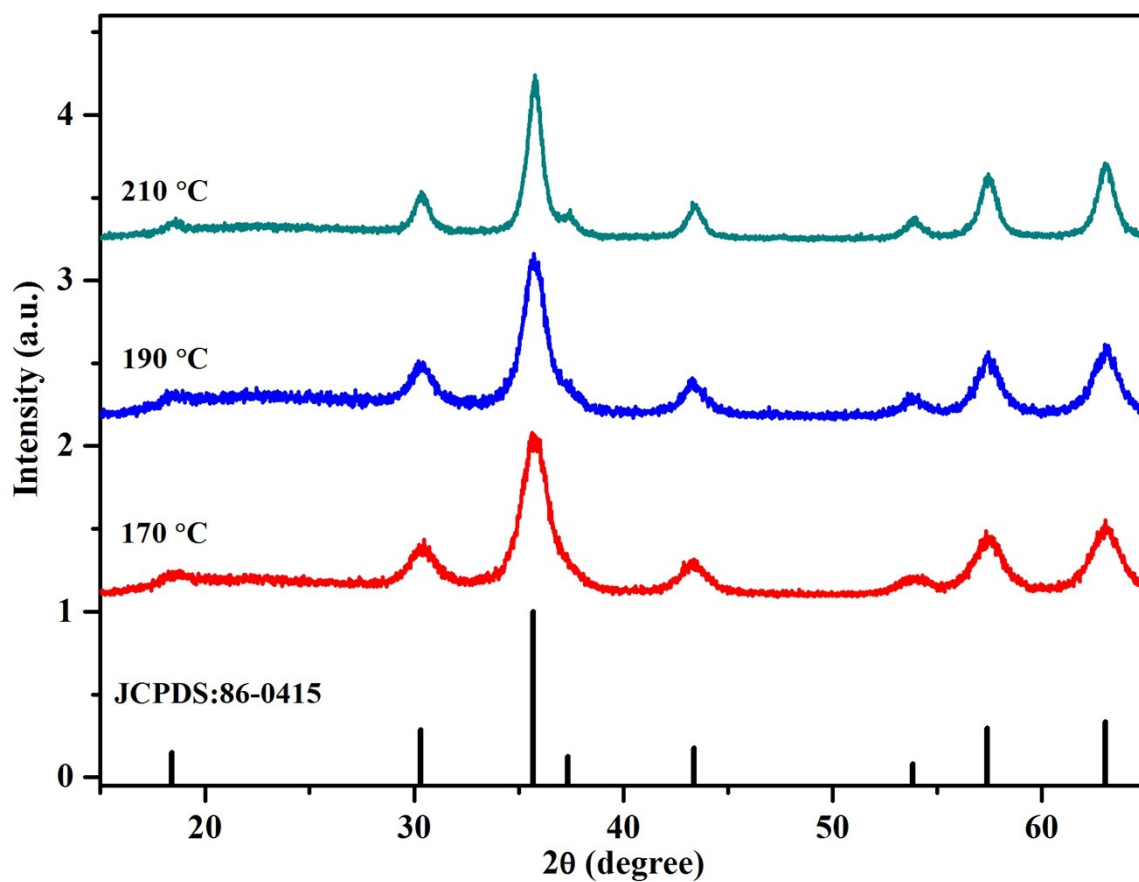


Figure S3. XRD patterns of ZnGa₂O₄:0.4%Cr³⁺ PLNPs synthesized at different temperatures for 16 h. All diffraction peaks match well with the standard pattern of cubic-phase ZnGa₂O₄ (JCPDS No. 86-0415), indicating pure phase and high crystallinity of the resulting PLNPs. The narrowing in the diffraction peaks with the rise of reaction temperature is attributed to the increase in the PLNP size, which agrees well with their size distribution acquired from TEM images.

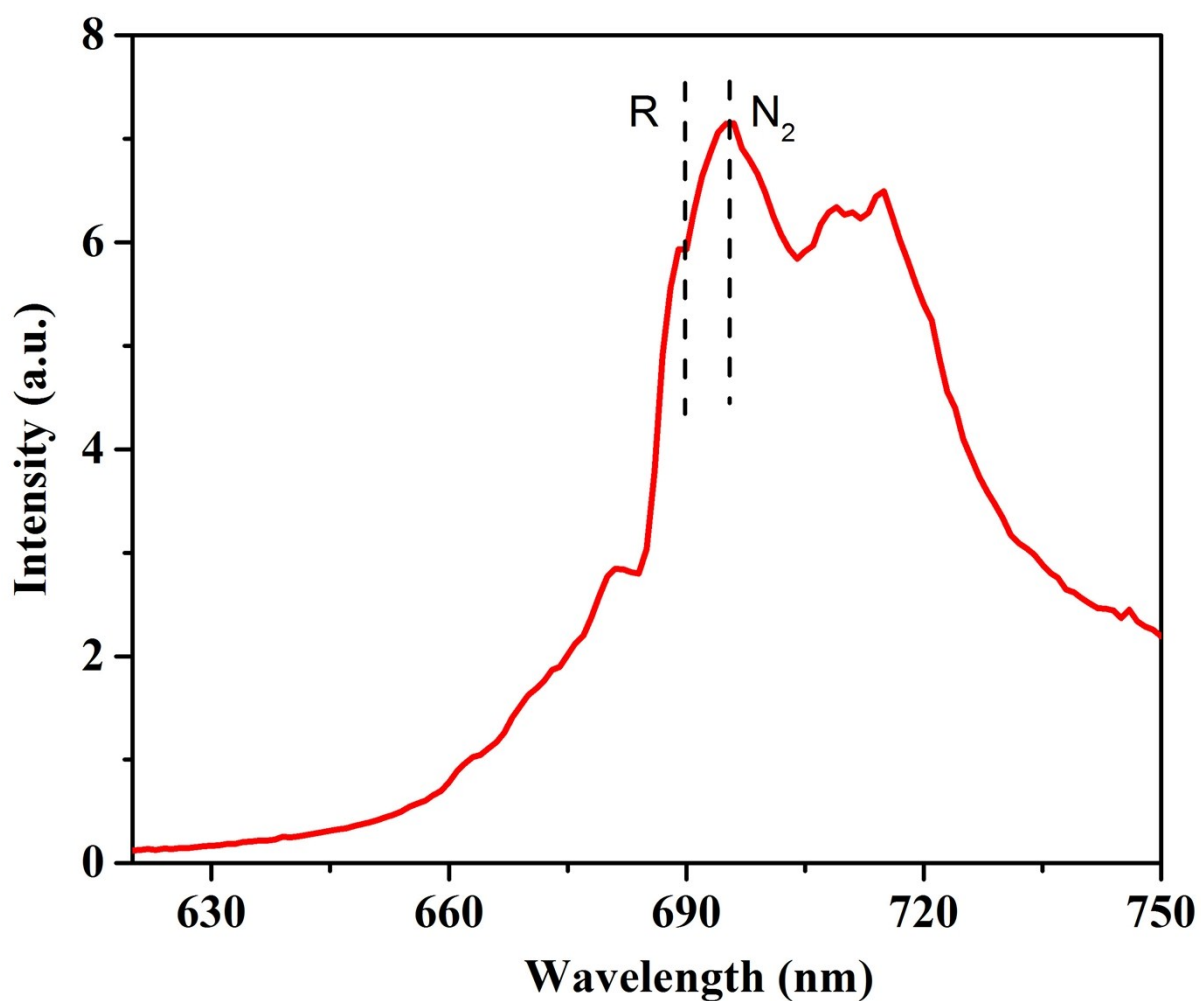


Figure S4. PL emission spectrum of $\text{ZnGa}_2\text{O}_4:0.4\%\text{Cr}^{3+}$ PLNPs under UV excitation at 271 nm. The emission peak at 695 nm labeled as N_2 line can be ascribed to the spin-forbidden ${}^2\text{E} \rightarrow {}^4\text{A}_2$ transition of Cr^{3+} occupying the much distorted octahedral site located in the first cationic neighbors of Cr^{3+} . The other relatively weak peaks could be attributed to the zero-phonon R lines and their associated phonon side bands.

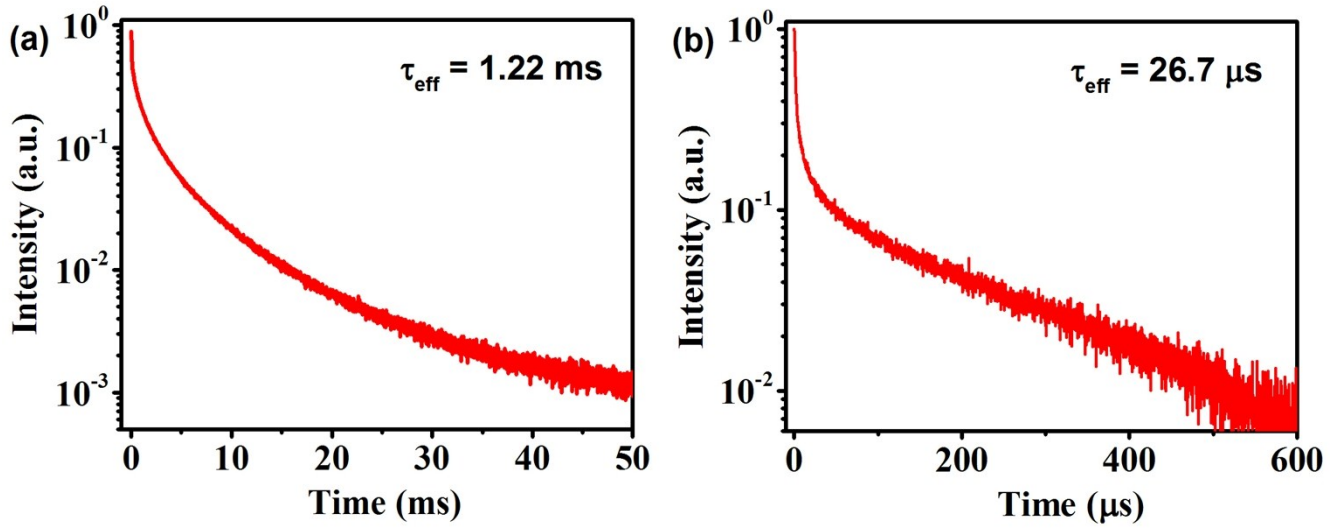


Figure S5. PL decays from (a) 2E and (b) 4T_2 of Cr^{3+} in $\text{ZnGa}_2\text{O}_4:0.4\%\text{Cr}^{3+}$ PLNPs by monitoring the Cr^{3+} emission at 695 nm and 730 nm, respectively. The effective PL lifetime was determined by

$$\tau_{\text{eff}} = \frac{1}{I_{\text{max}}} \int_0^{\infty} I(t) dt$$

where $I(t)$ denotes the PL intensity as a function of time t , and I_{max} represents the maximum PL intensity. The PL lifetimes of 2E and 4T_2 of Cr^{3+} were determined to be 1.22 ms and 26.7 μs , respectively. The PL lifetimes in the range of millisecond and microsecond for 2E and 4T_2 of Cr^{3+} , are typical of spin-forbidden and spin-allowed transitions from these two levels to the ground state 4A_2 of Cr^{3+} , respectively.

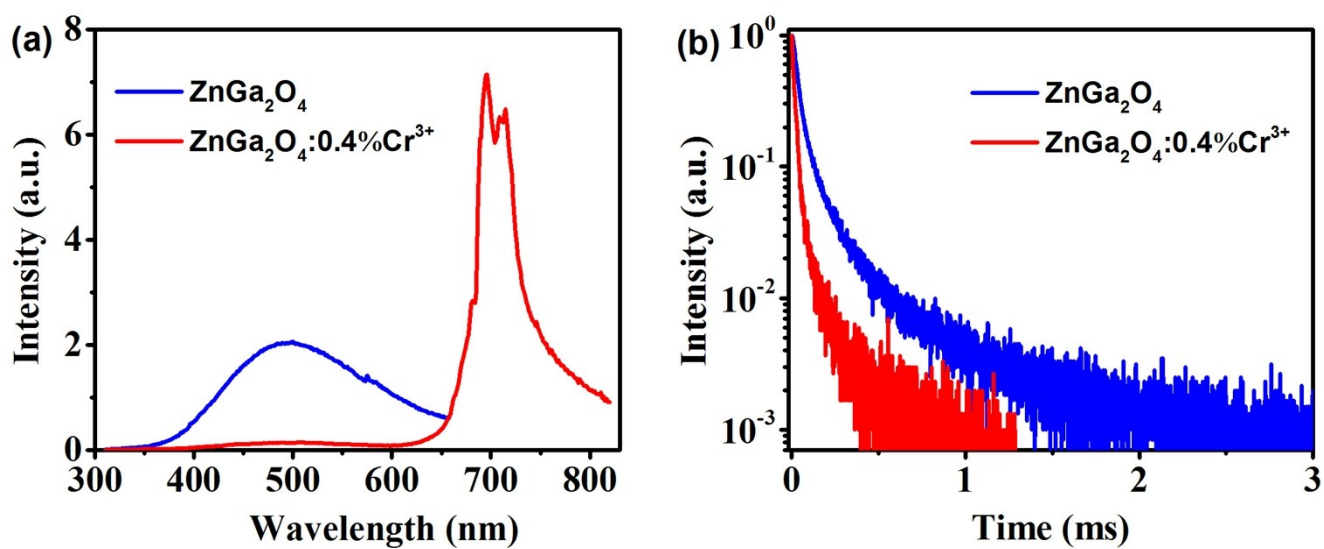


Figure S6. (a) PL emission spectra of ZnGa₂O₄ and ZnGa₂O₄:0.4%Cr³⁺ PLNPs upon UV excitation at 271 nm. (b) PL decays of ZnGa₂O₄ and ZnGa₂O₄:0.4%Cr³⁺ PLNPs by monitoring the host-related defect emission at 500 nm upon UV excitation at 271 nm. The effective PL lifetimes were determined to be 73.6 μ s and 19.7 μ s for ZnGa₂O₄ and ZnGa₂O₄:0.4%Cr³⁺, respectively.

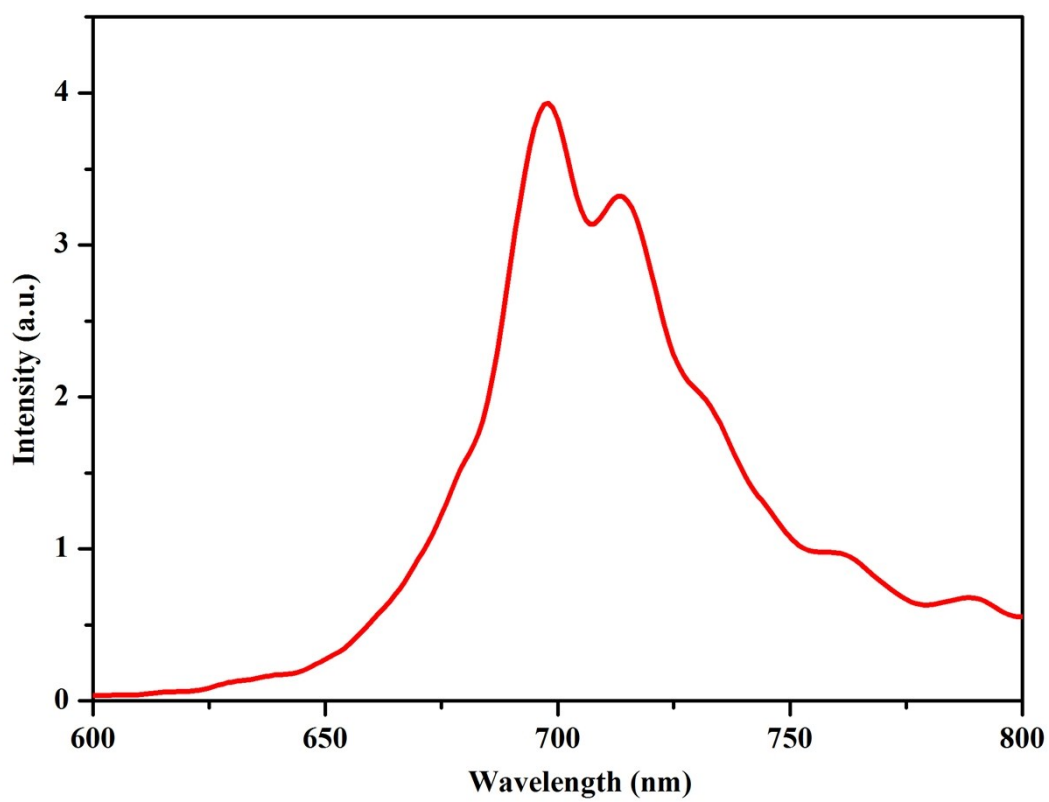


Figure S7. Afterglow emission spectrum of ZnGa₂O₄:0.4%Cr³⁺ PLNPs recorded at 1 min after the cease of excitation.

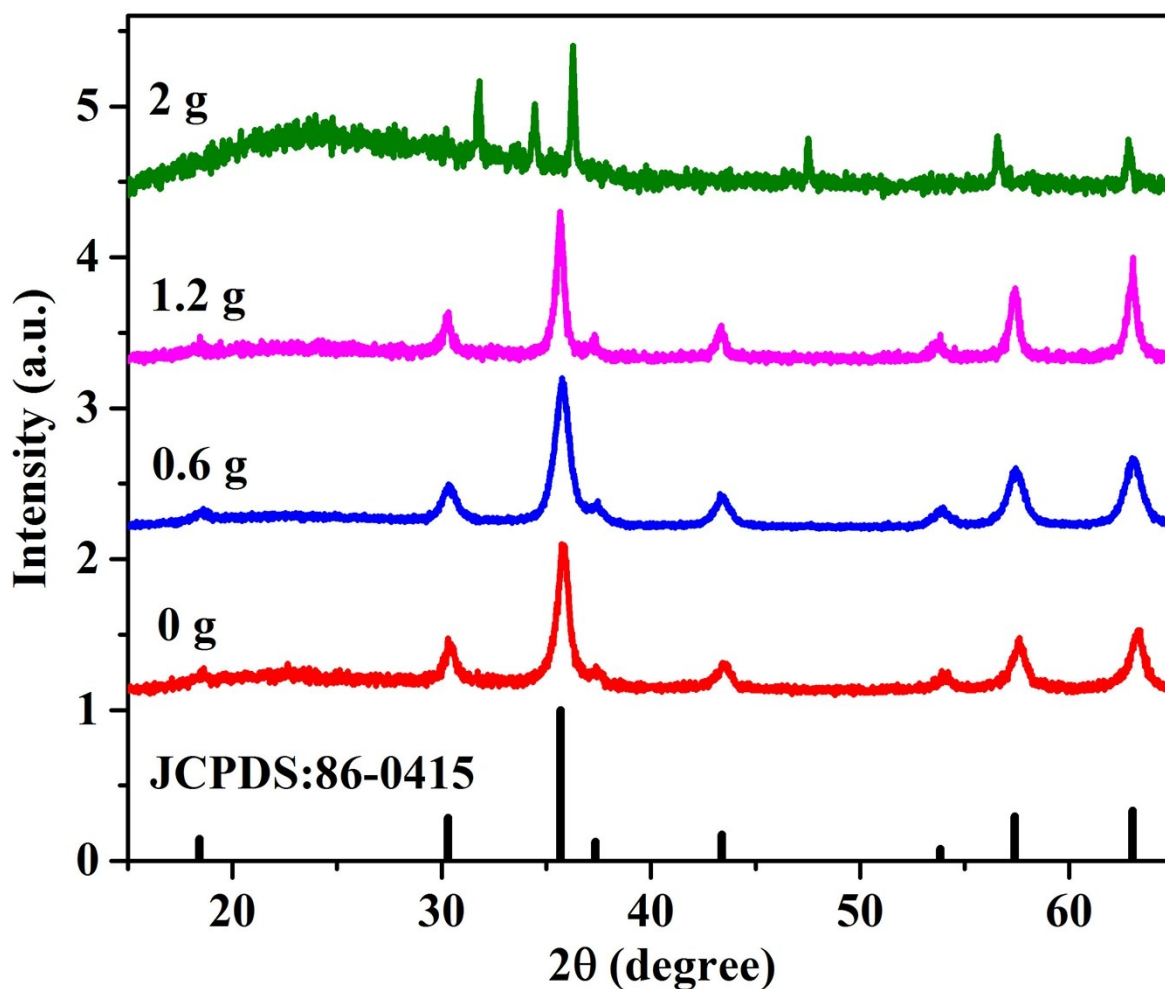


Figure S8. XRD patterns of ZnGa₂O₄:0.4%Cr³⁺ PLNPs synthesized with different amounts (0, 0.6, 1.2, 2 g) of NaOH in the precursor solution. The vertical lines represent the standard pattern of cubic-phase ZnGa₂O₄ (JCPDS No. 086-0415). All the diffraction peaks can be well indexed into cubic ZnGa₂O₄, except for the PLNPs synthesized with 2 g of NaOH. This indicates that the amount of NaOH in the synthesis has no significant influence on the size and phase of the resulting PLNPs.

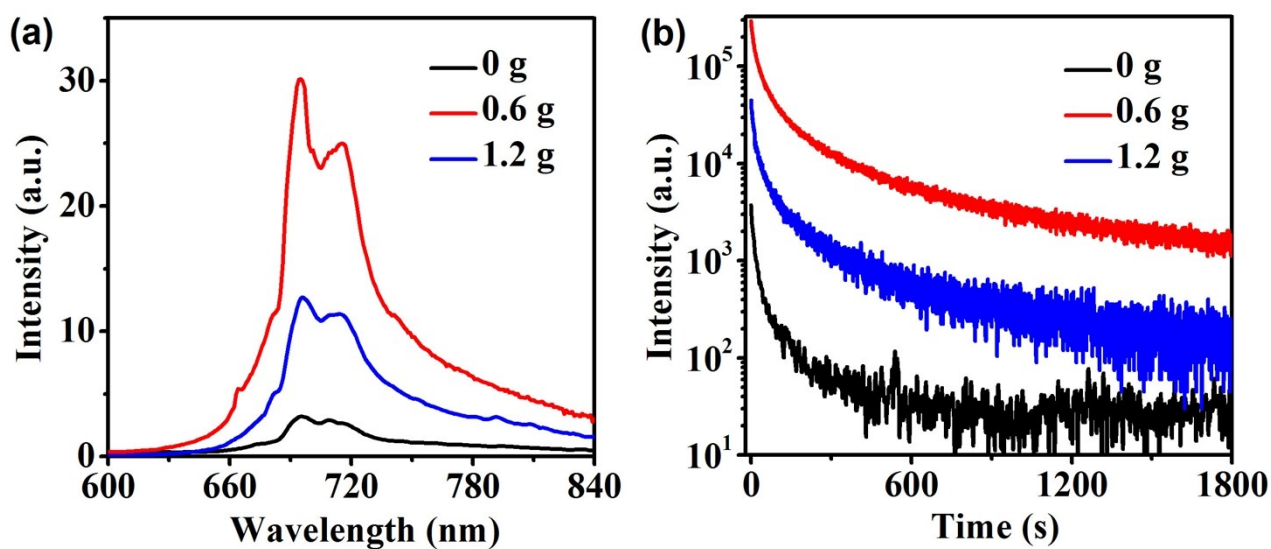


Figure S9. (a) RT PL emission spectra of ZnGa₂O₄:0.4%Cr³⁺ PLNPs synthesized with different amounts (0, 0.6, 1.2 g) of NaOH under UV excitation at 271 nm, and (b) their corresponding afterglow decay curves by monitoring the Cr³⁺ emission at 695 nm upon 254-nm UV lamp illumination for 5 min. It was found that the presence of NaOH in the synthesis was essential to improving the PL and afterglow properties of the resulting PLNPs.

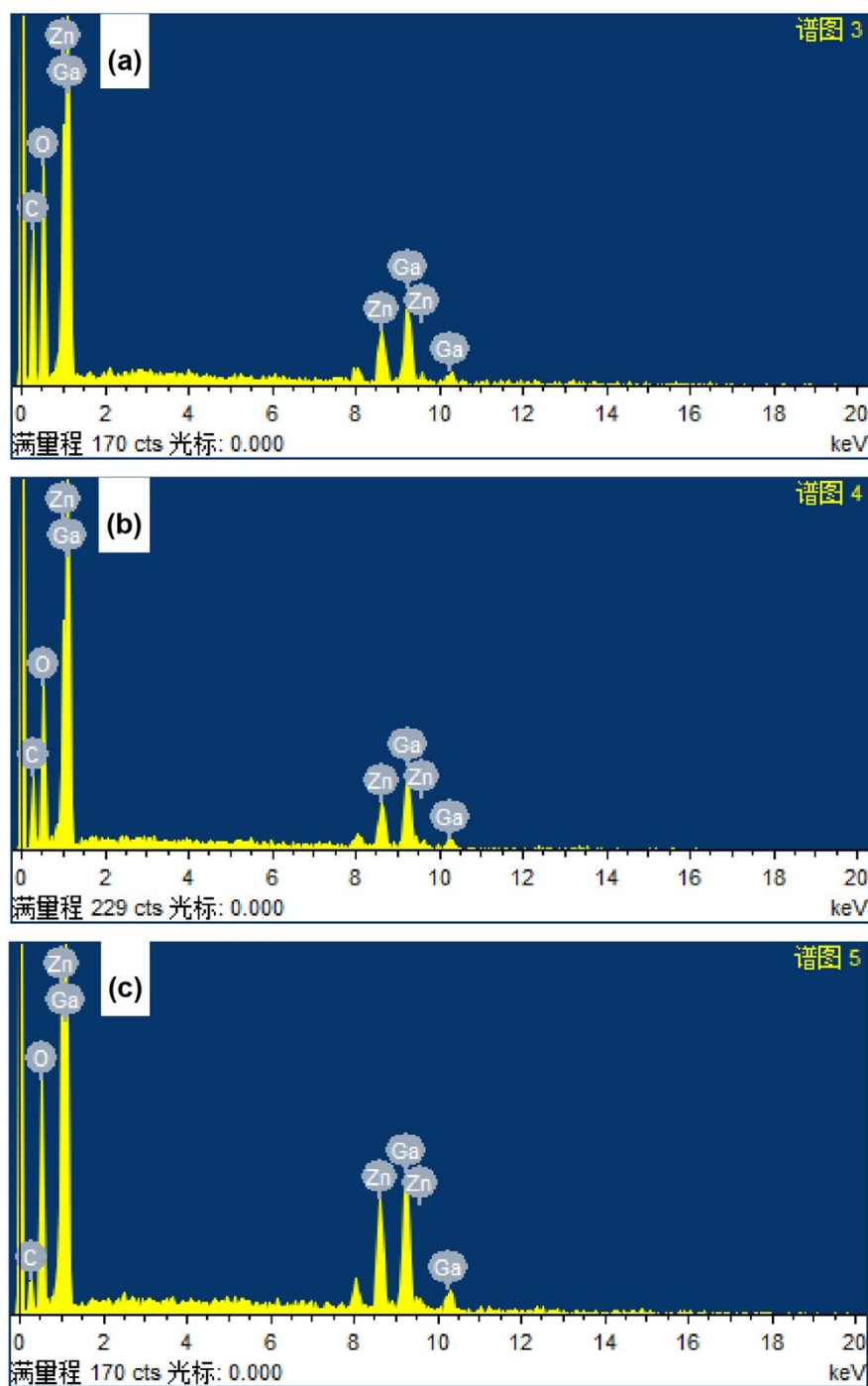


Figure S10. EDS patterns of ZnGa₂O₄:0.4%Cr³⁺ PLNPs synthesized with different amounts (0, 0.6, 1.2 g) of NaOH. Na signal was hardly detectable in EDS for all the PLNPs. In view of the large amount of NaOH in the synthesis, we deduced that Na⁺ did not enter into the lattice of ZnGa₂O₄.

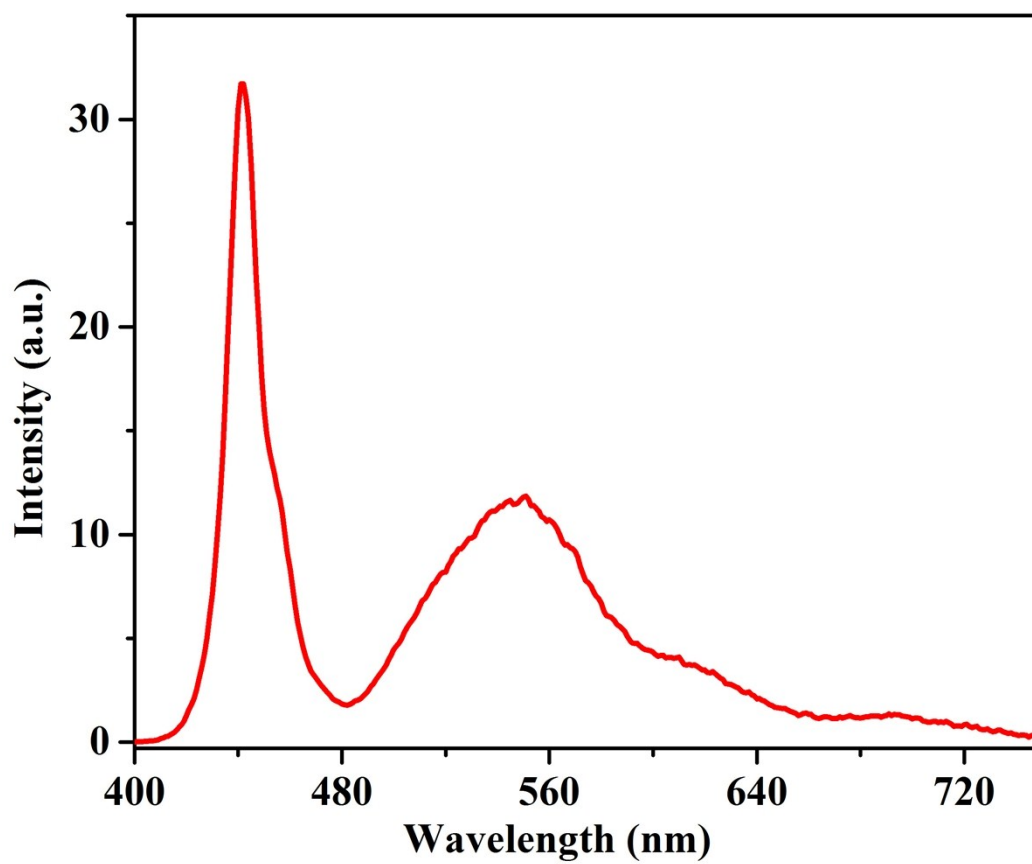


Figure S11. Emission spectrum of the white-light LED used as excitation source for $\text{ZnGa}_2\text{O}_4:0.4\%\text{Cr}^{3+}$ PLNPs.

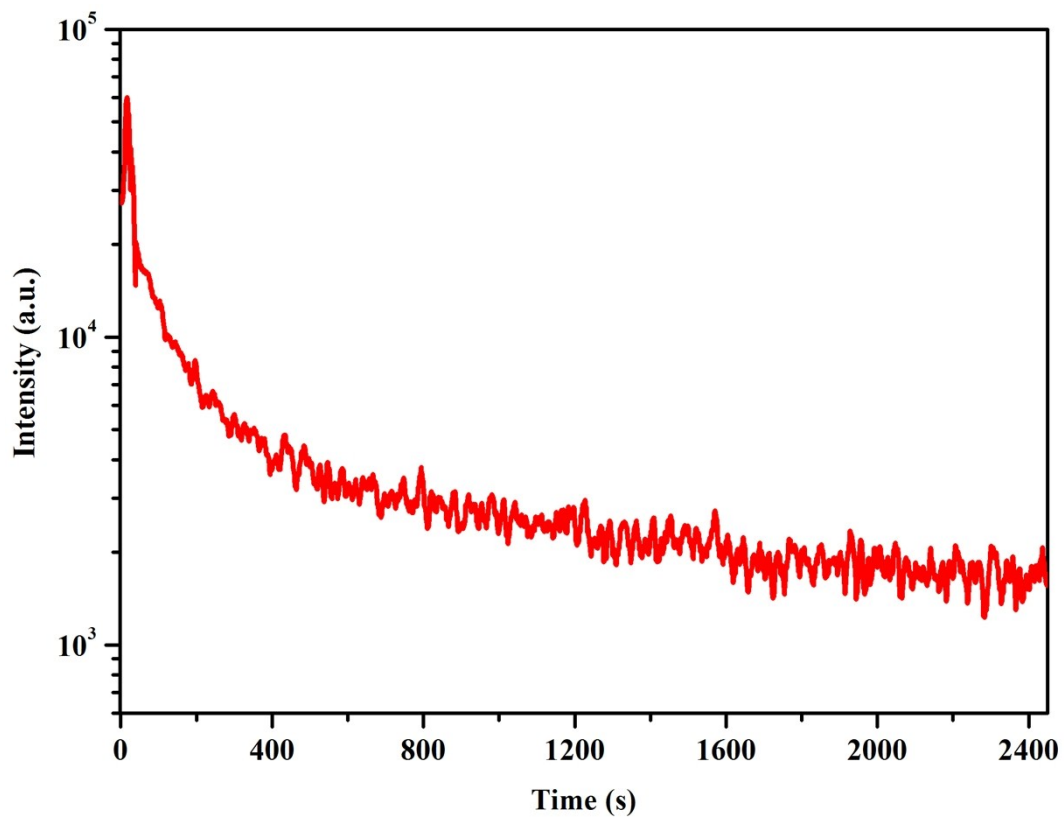


Figure S12. Afterglow decay curve of ZnGa₂O₄:0.4%Cr³⁺ PLNPs recorded at 77 K by monitoring the Cr³⁺ emission at 695 nm upon 254-nm UV lamp illumination for 5 min.

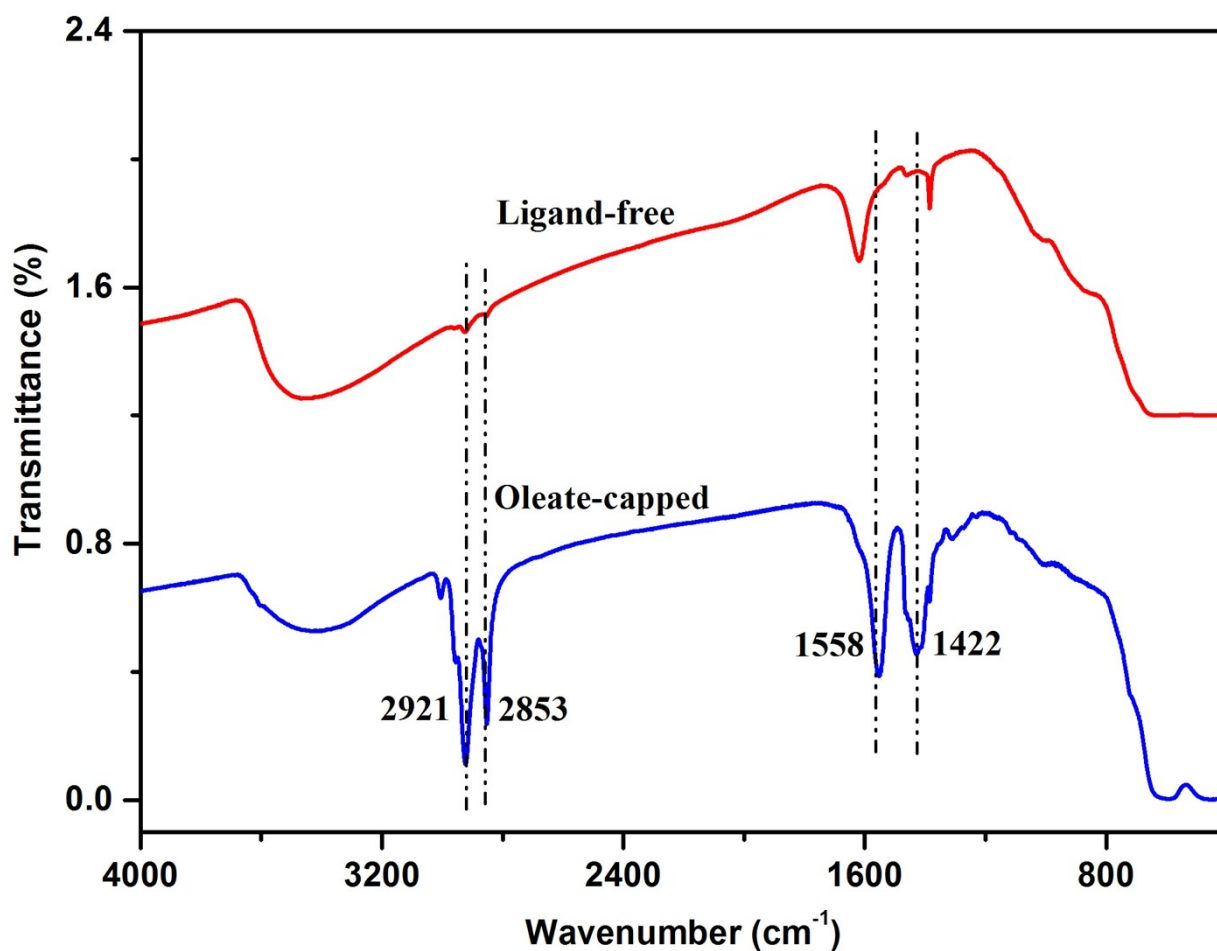


Figure S13. Fourier transform infrared (FTIR) spectra of oleate-capped and ligand-free $\text{ZnGa}_2\text{O}_4:0.4\%\text{Cr}^{3+}$ PLNPs. The original asymmetric and symmetric stretching vibrations of methylene ($-\text{CH}_2-$) in the long alkyl chain peaking at 2921 and 2853 cm^{-1} , and the asymmetric and symmetric stretching vibrations of carboxyl ($-\text{COO}^-$) peaking at 1558 and 1422 cm^{-1} in oleate-capped PLNPs disappeared for ligand-free PLNPs, indicating the successful removal of oleic ligands from the surface of the PLNPs.

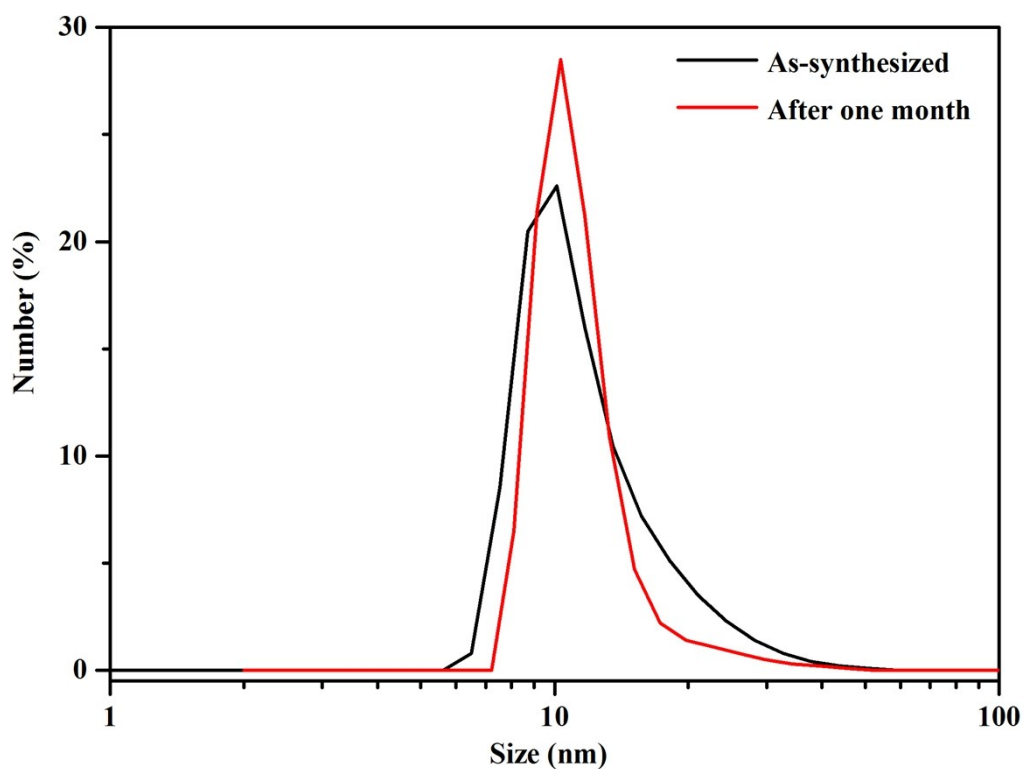


Figure S14. Hydrodynamic diameter distribution of the as-synthesized ligand-free $\text{ZnGa}_2\text{O}_4:0.4\%\text{Cr}^{3+}$ PLNPs dispersed in distilled water before and after their storage for one month. The hydrodynamic diameter of the as-synthesized ligand-free PLNPs was determined to be 10.1 nm, while after one month of storage it remained nearly unchanged with a value of 10.3 nm, indicative of the high stability of ligand-free PLNPs in distilled water.

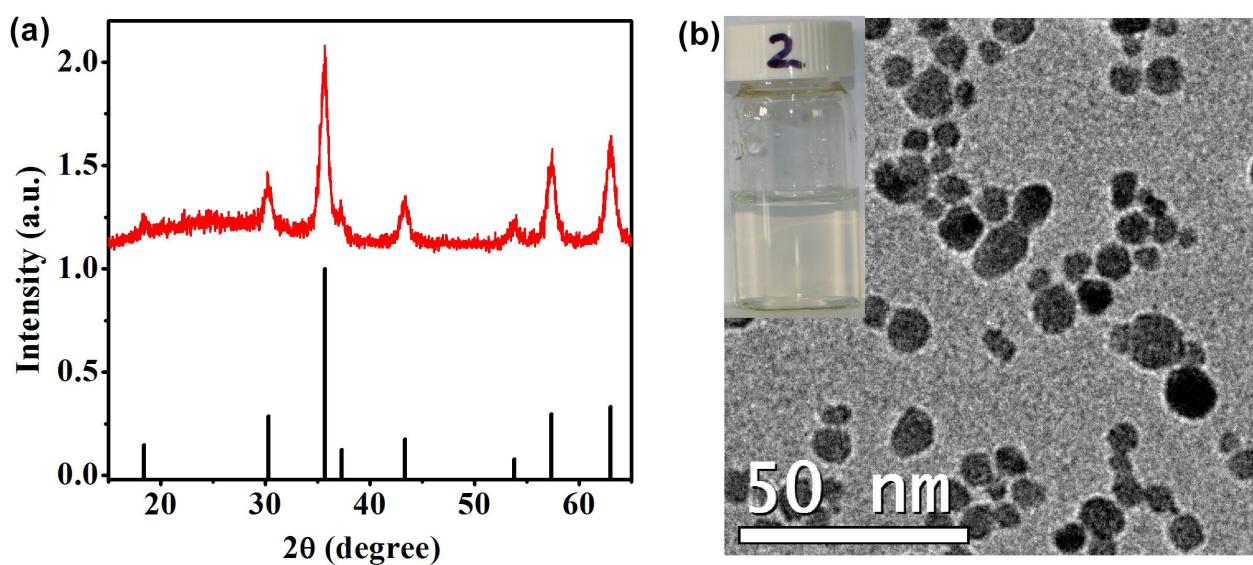


Figure S15. (a) XRD pattern and (b) TEM image of ligand-free $\text{ZnGa}_2\text{O}_4:0.4\%\text{Cr}^{3+}$ PLNPs. The photograph in the inset of (b) shows the transparency of ligand-free PLNPs dispersed in distilled water.

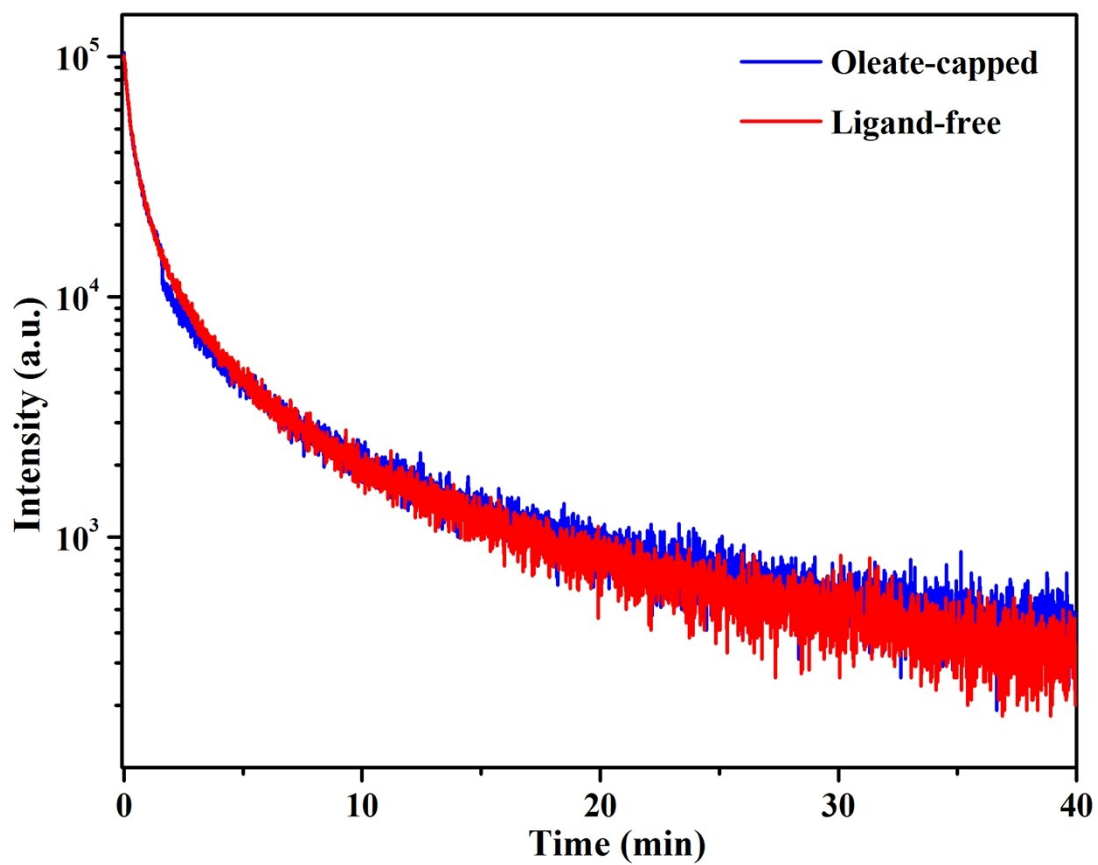


Figure S16. Afterglow decay curves of oleate-capped and ligand-free ZnGa₂O₄:0.4%Cr³⁺ PLNPs by monitoring the Cr³⁺ emission at 695 nm upon 254-nm UV lamp illumination for 5 min.

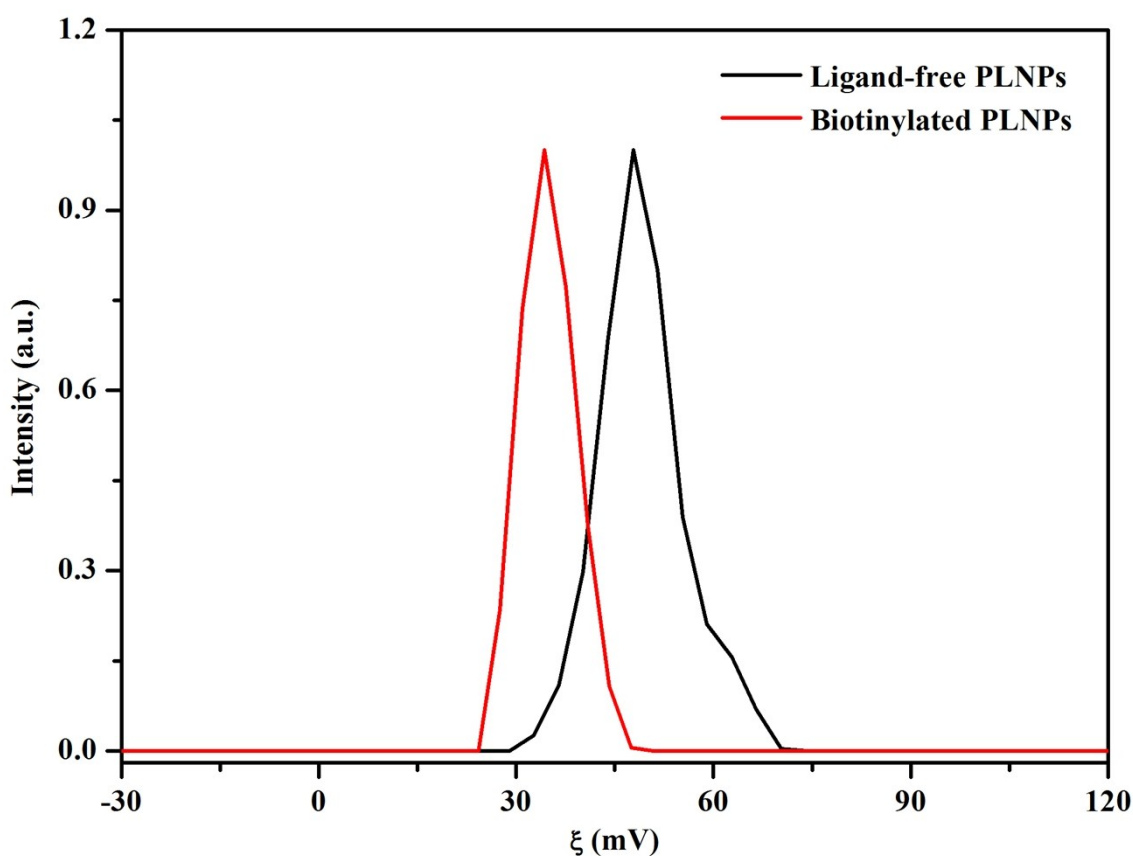


Figure S17. Zeta potentials of ligand-free and biotinylated $\text{ZnGa}_2\text{O}_4:0.4\%\text{Cr}^{3+}$ PLNPs obtained from the dynamic light scattering measurement. The zeta potential for ligand-free PLNPs dispersed in distilled water (pH=6.9) was determined to be +47.8 mV, which can be attributed to the positively charged $\text{Zn}^{2+}/\text{Ga}^{3+}$ ions exposed on the surface of ligand-free PLNPs. For comparison, the zeta potential of biotinylated PLNPs decreased from +47.8 mV to +34.3 mV, as a result of reduced positively charged $\text{Zn}^{2+}/\text{Ga}^{3+}$ ions exposed on the surface, thus confirming the successful conjugation of biotin to the surface of the PLNPs.

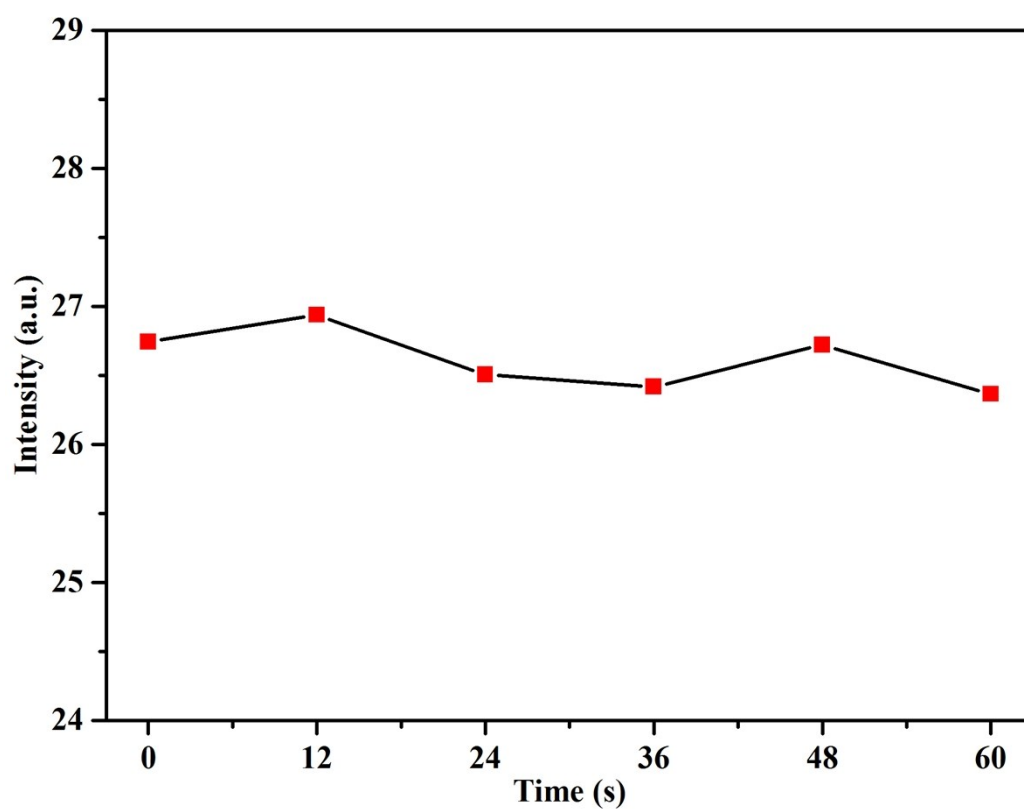


Figure S18. Afterglow signal of ligand-free $\text{ZnGa}_2\text{O}_4:0.4\%\text{Cr}^{3+}$ PLNPs measured on a multimodal microplate reader (Synergy 4, BioTek). Each data point represents the afterglow signal of the PLNPs with identical concentration in each well of the 96-well microplate. The integrating time was set as 2 s and the time interval for the measurement of each well of the 96-well microplate was set as 10 s.

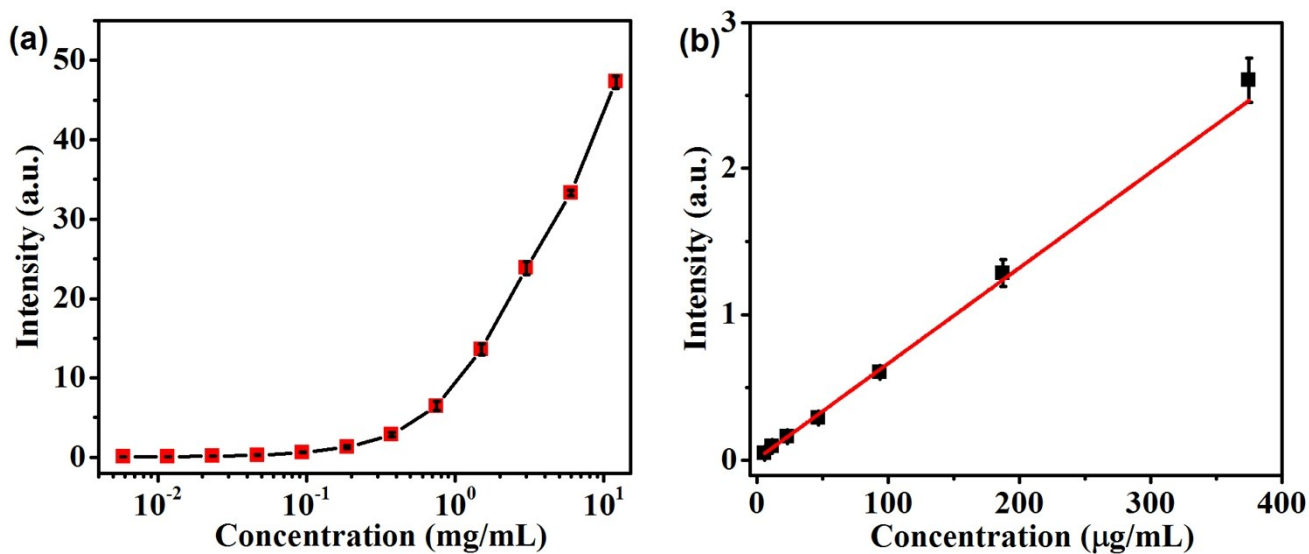


Figure S19. (a) Concentration-dependent afterglow signal of ligand-free ZnGa₂O₄:0.4%Cr³⁺ PLNPs dissolved in distilled water. (b) The linear range of the afterglow signal *versus* the PLNP concentration (0-375 µg/mL). Each data point represents the mean (\pm standard deviation) of three independent experiments.

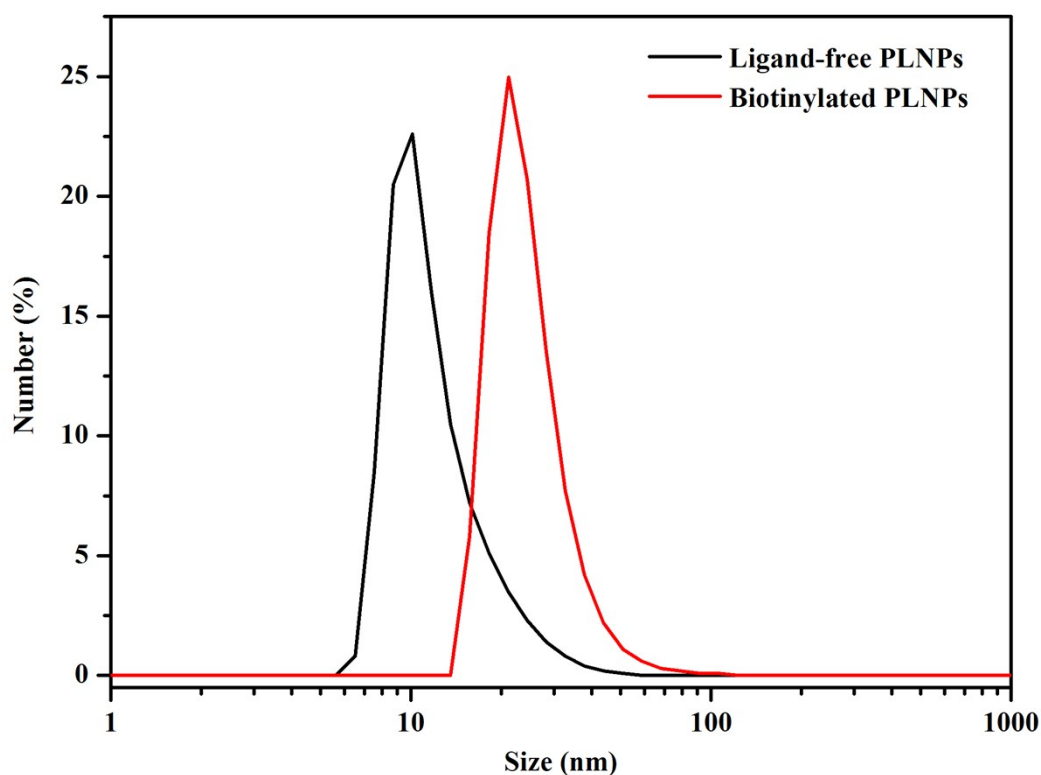


Figure S20. Hydrodynamic diameter distribution of ligand-free and biotinylated $\text{ZnGa}_2\text{O}_4:0.4\%\text{Cr}^{3+}$ PLNPs dispersed in distilled water. The hydrodynamic diameters of ligand-free and biotinylated PLNPs were determined to be 10.1 nm and 21.1 nm, respectively. The increase in the hydrodynamic diameter of biotinylated PLNPs as compared to that of their ligand-free counterparts is attributed to the conjugation of biotin to their surface that may cause aggregation of the PLNPs.